Upconversion red emission and Near-infrared quantum-cutting persistent luminescence of Nd^{3+} activated Ca_2SnO_4 induced by Yb^{3+}

Jing-Xiang Zhang[#], Dejian Hou[#], Jin-Yan Li, Huihong Lin[*], Rui Huang, Yi Zhang, Jianhua Hao[*]

Dr. J.-X. Zhang, Dr. J.-Y. Li, Prof. H.H. Lin[*]

School of Chemical and Environmental Engineering

Hanshan Normal University

Chaozhou 521041, Guangdong, P. R. China

E-mail: linhh@hstc.edu.cn

Dr. D.J. Hou, Y. Zhang, Prof. R. Huang

School of Materials Science and Engineering

Hanshan Normal University

Chaozhou 521041, Guangdong, P. R. China

Prof. J.H. Hao[*]

Department of Applied Physics

The Hong Kong Polytechnic University

Hong Kong, P. R. China

E-mail: jh.hao@polyu.edu.hk

[#] These authors contributed equally and served as co-first authors.

Keywords: near-infrared luminescence, upconversion, quantum cutting, persistence

In this work, we have investigated the steady-state and time-resolved near-infrared (NIR) photoluminescence (PL), upconversion (UC) and long-lasting phosphorescence (LLP)

properties in the Nd^{3+}/Yb^{3+} doped Ca_2SnO_4 samples. Two-photon NIR quantum cutting (QC) luminescence is observed when the Nd^{3+}-O^{2-} charge-transfer band (CTB) in Ca_2SnO_4: Nd^{3+}, Yb^{3+} phosphors was excited. More interestingly, the unique two-photon UC red emission under 808 nm laser diode excitation and NIR QC persistent luminescence can be realized only in Nd^{3+}-Yb^{3+} co-doped samples. The energy transfer mechanism between Nd^{3+} and Yb^{3+} is revealed from energy level and decay measurements. Different cross relaxation schemes related to $^2F_{5/2}$-$^2F_{7/2}$ of Yb^{3+} and *f-f* transition of Nd^{3+} are proposed. The results show that the multimode luminescent properties have achieved in Nd^{3+}-doped Ca_2SnO_4 with the introduction of Yb^{3+}.

1. Introduction

In the last decade, NIR luminescent materials are widely developed to promote their applications in photovoltaics, laser, optical communication, infrared photon counter, bio-imaging *in vivo*, etc.[1-5] Among these NIR materials, the more concerned is the NIR QC and NIR LLP phosphors due to their outstanding contributions in energy and biology fields.[6-13] Meijerink et al. firstly reported the NIR QC of Tb^{3+}-Yb^{3+} co-doped YPO_4.[6] The theoretical quantum yield reaches up to 188% on the basis of cooperative QC dynamics. It is proposed that the application of cooperative energy transfer (CET) has prospects for increasing the energy efficiency of crystalline Si solar cells by photon doubling of the high energy part of the solar spectrum. Moreover, Pan et al. reported a new NIR LLP process called up-converted persistent luminescence (UCPL) in $Zn_3Ga_2GeO_8$: Cr^{3+}, Yb^{3+}, Er^{3+} (ZGGO: Cr, Yb, Er) phosphors.[9] After being excited by a 980 nm laser, the phosphor emits long-lasting (>24 h) NIR persistent emission peaking at 700 nm. Superior NIR persistent luminescence property enable the ZGGO: Cr, Yb, Er phosphor to find application in biomedical imaging field. By combining the features of QC and LLP luminescence, Wang et al. reported the first NIR QC LLP phosphor $Ca_2Ga_2GeO_7$:Pr^{3+},Yb^{3+}, incorporating acceptor Yb^{3+} ions into the LLP

phosphor $Ca_2Ga_2GeO_7:Pr^{3+}$.[11] These materials are expected to have important implications for several fields such as crystalline Si solar cells and biomedical imaging.

The electronic configuration of Nd^{3+} is [Xe]$4f^3$. As the energy levels derived from the $4f^3$ configuration are well shielded from the crystal field, there is only slight variation in the laser wavelengths from one host crystal to another. The energy level structure of Nd^{3+} shows a multitude of levels, and many of them are emissive.[14,15] Generally, Nd^{3+} ion is considered as a good candidate in UC systems for improving the pumping efficiency of 808 nm laser diode, due to its large absorption cross-section around 800 nm.[16] The Nd^{3+}-doped oxide glasses and crystals are always attracted as solid-state lasers with NIR dominated emission at about 1064 nm which is assigned to the $^4F_{3/2}$- $^4I_{11/2}$ transition.[17-19] Our previous work indicated that dual-mode functions of NIR-to NIR UC or NIR-to-NIR DS (downshifting) have been realized in Nd^{3+} singly doped KY_3F_{10} under 808 nm laser excitation and NIR LLP luminescent properties have been achieved in Nd^{3+}: $Ca_3Ga_2Ge_3O_{12}$ phosphors.[20,21] Therefore, the spectroscopic properties including UC, DS and LLP of Nd^{3+} in different host lattices are necessary not only for basic research but also for possible application.

Much current interest has been focused on tuning multimodal luminescence to improve the phosphors luminescence properties and developing new inorganic phosphors with high chemical stability and intense luminescence.[22-24] The host Ca_2SnO_4 has been considered to be one of the most promising and suitable materials for long persistent luminescence, because of its one-dimensional chains structure. It is very easy to implant other ions into the host lattices, and generally exhibits special luminescence properties.[25-28] According to our current experiments, Nd^{3+}: Ca_2SnO_4 might only involve NIR DS ($\lambda_{em} \approx$ 905, 1083 and 1348 nm) luminescent properties. UC and LLP luminescence has not been observed in Nd^{3+} singly-doped Ca_2SnO_4. However, the addition of Yb^{3+} changed this phenomenon in the Nd^{3+}: Ca_2SnO_4 system. The two-photon UC red emission and NIR LLP luminescence can be obtained only in Nd^{3+}/Yb^{3+} co-doped Ca_2SnO_4. Besides, due to the introduction of Yb^{3+}, two-

photo NIR QC in Ca_2SnO_4: Nd^{3+}-Yb^{3+} phosphors occur. Motivated by these desires, we designed and synthesized a series of Nd^{3+} and Yb^{3+} co-doped Ca_2SnO_4 phosphors. In this work, the investigations on NIR QC, UC and LLP luminescence are presented in Ca_2SnO_4: Nd^{3+} and Ca_2SnO_4: Nd^{3+}, Yb^{3+} phosphors. More importantly, the energy transfer mechanisms between Nd^{3+} and Yb^{3+} are discussed. In particular, the NIR QC LLP luminescence process is revealed by cross-relaxation energy transfer from the traps level of Nd^{3+}/Yb^{3+} co-doped Ca_2SnO_4 to two Yb^{3+} ions.

2. Results and Discussion

2.1. Structure and phase characterizations

Phase identification of a series phosphors $Ca_{2-x}Nd_xSnO_4$ (x = 0, 0.0025, 0.005, 0.01, 0.03, 0.05, 0.1) and $Ca_{1.99-y}Nd_{0.01}Yb_ySnO_4$ (y = 0.01, 0.03, 0.05, 0.1, 0.15) were measured. As examples, Figure 1(a) displays the XRD patterns with chemical formulas Ca_2SnO_4, $Ca_{1.99}Nd_{0.01}SnO_4$, and $Ca_{1.89}Nd_{0.01}Yb_{0.1}SnO_4$, respectively. All the samples were found to be pure single phase (JCPDS 70-2404), which suggests that the nominal substitutions of Ca^{2+} by Nd^{3+}/Yb^{3+} have little influence on the host crystal structure.

The structure of Ca_2SnO_4 belongs to the Sr_2PbO_4-type.[25] Calcium atom is at the *4h* site and coordinated by seven oxygen atoms, and the Sn atom of the *2a* site is coordinated by six oxygen atoms. There are two oxygen sites, locate at *4h* site and *4g* site, respectively. The structure is comprised of one-dimensional chains of edge-sharing octahedral, in which the terminal Sn-O bonds are shorter than the equatorial Sn-O bonds, as shown in Figure 1(b). The approximate ionic radii of Ca^{2+} and Sn^{4+} cations in Ca_2SnO_4 are as follows: Ca^{2+} on 7-coordinated site (CN = 7, r = 1.06 Å); Sn^{4+} on 6-coordinated site (CN = 6, r = 0.69 Å). In Ca_2SnO_4 matrix, the most concerned phosphor is that Eu^{3+}-doped Ca_2SnO_4 exhibits strong photoluminescence derived from the $^5D_0$-$^7F_2$ electric dipole transition of Eu^{3+} together with afterglow emissions at RT.[26] It was reported that Eu^{3+} ion was substituted at both Ca^{2+} and

Sn^{4+} sites in the host lattice, and the Sn^{4+} site had created several hole traps for luminescence by Eu^{3+} ion substitution.[27] However, in Eu^{3+}-Y^{3+} co-doped Ca_2SnO_4, Y^{3+} ions with a smaller ionic radius preferentially occupy smaller cation (Sn^{4+}) sites, driving larger Eu^{3+} ions out of the Sn^{4+} site into the larger Ca^{2+} site.[28] As described above, considering their ionic radii, it is logical to assume that the Nd^{3+} (whose ionic radii are 1.11 and 0.98 Å when 8- and 6-coordinated with oxygen) preferentially occupy the Ca^{2+} sites while the smaller Yb^{3+} (0.92 Å for CN=7 and 0.87 Å for CN=6) may partially occupy smaller Sn^{4+} sites to keep the charge balance in Nd^{3+}/Yb^{3+} co-doped Ca_2SnO_4. More details will be discussed in the following sections.

2.2. The NIR luminescent properties of Nd^{3+} in Ca_2SnO_4

Figure 2(a) depicts the luminescence spectra of the $Ca_{1.99}Nd_{0.01}SnO_4$ sample at RT. Under 266 nm (attributed to Nd^{3+}-O^{2-} CTB) ultraviolet light excitation, three groups of emission bands located at 890 ~950 nm, 1050 ~1150 nm and 1320 ~1430 nm can be observed (curve i), which are ascribed to the electron transitions from the excited state $^4F_{3/2}$ to the ground state ^4I_J (J = 9/2, 11/2 and 13/2) of Nd^{3+} ions. The most intense emission is around 1083 nm assigned to Nd^{3+} $^4F_{3/2}$- $^4I_{11/2}$ transition. By monitoring the emission peak at 1083 nm, the corresponding excitation spectrum is achieved (curve ii). The excitation spectrum contains a series of sharp peaks, attributing to the transitions from $^4I_{9/2}$ ground state to the excited states like $^4G_{11/2}$,$^4G_{9/2}$,$^2G_{7/2}$, $^4G_{5/2}$, $^4F_{7/2}$, $^4F_{5/2}$ of Nd^{3+}.

In addition, a broad band peaked at about 260 nm (~4.77 eV) can be observed in excitation spectrum, which is probably attributed to Nd^{3+}-O^{2-} CTB.[29] Generally speaking, the trivalent ions (Nd^{3+}, Sm^{3+}, Eu^{3+}, Yb^{3+} etc.) have a tendency to become divalent that show charge-transfer absorption bands in the ultraviolet. Further, it was reported that the excitation spectra of Ca_2SnO_4: Eu^{3+} phosphors display a broad peak at around 300 nm (~4.13 eV) of Eu^{3+}-O^{2-} CTB (250–350 nm).[26] According to the report of Dorenbos[30] that there is a

relationship correlation the CTB energies of Eu^{3+} and Nd^{3+} ions in the same lattice site of a specific host, which is described as:

$$E^{CT}(Nd^{3+}) = E^{CT}(Eu^{3+}) + (2.29 \pm 0.12)\ eV \quad (1)$$

where $E^{CT}(Nd^{3+})$ and $E^{CT}(Eu^{3+})$ are the energies of the charge transfer absorption bands of Nd^{3+} and Eu^{3+}, respectively. Using the equation (1), we predicted that the CTB of Nd^{3+}-O^{2-} in Ca_2SnO_4 would be 6.42 ± 0.12 eV, i.e., around 195 nm, thus showing a disagreement with our experimental results. But in the report, Dorenbos presented scarce the information on the E^{CT} values for Ce^{3+}, Pr^{3+}, Nd^{3+}, so we suspect the equation may not be generally applied to all samples. From the excitation spectra of Nd^{3+}/Yb^{3+} co-doped Ca_2SnO_4, shown in Figure 3(a), it can be determined that this ~260 nm band is really derived from Nd^{3+}-corrected transition, which can be reasonably considered as Nd^{3+}-O^{2-} CTB in this work.

Figure 2(b) shows the emission spectra of $Ca_{1.99}Nd_{0.01}SnO_4$ sample under 266 nm, 582 nm and 808 nm excitation, respectively. The main emission lines are similar for these three spectra, the integrate emission intensities of $Ca_{2-x}Nd_xSnO_4$(x = 0.0025, 0.005, 0.01, 0.03, 0.05, 0.1) under 808 nm excitation are displayed in the inset of Figure 2(b).We can see the optimal emission intensity occurs at x≈ 0.005-0.01, then the emission intensity decreases due to the concentration quenching effect. Based on the doping concentration, the critical energy transfer distance R_c between Nd^{3+} ions can be estimated by the following equation:[31]

$$R_c \approx 2\left(\frac{3V}{4\pi x_c N}\right)^{\frac{1}{3}} \quad (2)$$

where V is the volume of one unit cell, N is the number of Ca^{2+} ions in the unit cell, x_c is the critical concentration. In the present case, V = 181.87 Å^3, N = 4, therefore, R_c is calculated to be 18.72 Å. A value of R_c > 5 Å indicates that multipolar interactions are dominant. A dipole−dipole mechanism appears most probable because both donor and acceptor transitions are electric dipole allowed.

Figure 2(c) illustrates the decay curves of $Ca_{2-x}Nd_xSnO_4$ (x = 0.0025, 0.005, 0.01, 0.03, 0.05, 0.1) under 808 nm excitation, the decay curves almost overlap with each other for x = 0.0025 and 0.005 samples, but the decay process becomes faster from x = 0.01, which is due to the interaction or energy migration between Nd^{3+} ions. The decay curves further confirm the concentration quenching effect in the system.

2.3. The NIR QC luminescence in Nd^{3+}/Yb^{3+} co-doped Ca_2SnO_4

As an example of the spectra of the series $Ca_{1.99-y}Nd_{0.01}Yb_ySnO_4$ (y = 0.01, 0.03, 0.05, 0.1, 0.15), the room-temperature UV-Vis-NIR excitation and NIR emission spectra of $Ca_{1.89}Nd_{0.01}Yb_{0.1}SnO_4$ are displayed in Figures 3 and 4.

As we know, Yb^{3+} has the $4f^{13}$ configuration and two groups of energy levels $^2F_{5/2}$ and $^2F_{7/2}$, the separation between the $^2F_{5/2}$ and $^2F_{7/2}$ levels are around 10 000 cm^{-1}. When monitoring the emissions at ~1003 (Yb^{3+} emission) and ~1083 nm (Nd^{3+} emission), both curves exhibit similar absorptions from Nd^{3+} in Figure 3(a). In order to clearly observe the effect of CTB absorption on $^4D_{3/2}$ population, we normalized the excitation peak at 602 nm. Obviously, efficient energy transfer from $Nd^{3+} \rightarrow Yb^{3+}$ occurs. It is well known that the emission of Nd^{3+} (in NIR region) and the absorption of Yb^{3+} (CTB maybe in the deep ultraviolet region) do not overlap, so the energy transfer cannot occur through the resonance process. Combining the emission spectra in the inset of Figure 4(a), we found that the NIR QC luminescence in Nd^{3+}/Yb^{3+} co-doped Ca_2SnO_4 occurs. So, it is inferred that the energy transfer between Nd^{3+} and Yb^{3+} may be a cross-relaxation or cooperative process.

From these two excitation spectra, we can obviously observe the population of $^4D_{3/2}$, $^4G_{5/2}$ and $^4F_{3/2}$ levels, peaking at about 367, 600, and 819 nm, respectively. More interestingly, a key observation was had the intensity of the ~262 nm band at 1003 nm emissions is significantly stronger than that at 1083 nm emission. Here, this absorption band may be ascribed to Nd^{3+}-O^{2-} CTB, which is consistent with that of Nd^{3+} singly-doped Ca_2SnO_4

(Figure 2a). This shows that there is a close relationship between Yb^{3+} emission and Nd^{3+}-O^{2-} CTB. In order to reveal the connection of Nd^{3+}-O^{2-} CTB and NIR QC luminescence, the energy-level diagram is schematically displayed in Figure 3(b), illustrating the proposed energy transfer mechanisms in Nd^{3+}/Yb^{3+} co-doped Ca_2SnO_4. Upon 262 nm excitation (Nd^{3+}-O^{2-} CTB), strong Yb^{3+} NIR emission and relatively weak Nd^{3+} emission are observed, as shown in the inset of Figure 4(a). It is understandable that the energy transfer occurs from Nd^{3+} to Yb^{3+} via two-step cross-relaxation between $^4D_{3/2}$–$^4I_{9/2}$ of Nd^{3+} and $^2F_{5/2}$–$^2F_{7/2}$ transition of Yb^{3+} and two-step nonradiative relaxation processes. It is possible that energy transfer firstly occurs via nonradiative relaxation from the level of Nd^{3+}-O^{2-} CTB to $^4D_{3/2}$. Then, it is reasonable that cross-relaxation processes are as follows:

$$Nd^{3+}\ (^4D_{3/2}) + Yb^{3+}\ (^2F_{7/2}) \rightarrow Nd^{3+}\ (^4G_{5/2}) + Yb^{3+}\ (^2F_{5/2})\ \text{(marked as ET1)} \quad (3)$$

$$Nd^{3+}\ (^4F_{3/2}) + Yb^{3+}\ (^2F_{7/2}) \rightarrow Nd^{3+}\ (^4I_{9/2}) + Yb^{3+}\ (^2F_{5/2})\ \text{(marked as ET2)} \quad (4)$$

Another nonradiative relaxation process take place from $^4G_{5/2}$ to $^4F_{3/2}$ in the course. Finally, the two-photon NIR QC luminescence occurs under an excitation at Nd^{3+}-O^{2-} CTB in Nd^{3+}/Yb^{3+} co-doped Ca_2SnO_4. Compared with the previously reported NIR QC system, the NIR QC efficiency in Nd^{3+}/Yb^{3+} co-doped Ca_2SnO_4 can be improved due to a larger CTB absorption cross section. At present, the shortcomings of the practical application of NIR QC is that the activator Ln^{3+} (Ln = Tm, Er, Ho) has a small absorption cross-section, while it can enhance the absorption of activated ions in the ultraviolet-visible region to achieve enhanced NIR QC emission under broadband CTB excitation. Here, it is proposed that the application of CTB on NIR QC in Nd^{3+}/Yb^{3+} co-doped Ca_2SnO_4 has prospects for greatly increasing the energy efficiency of crystalline Si solar cells.

It is worth noting that these two excitation spectra have small difference, as marked with the dotted blue square in Figure 3(a). It can be observed that the excitation peak at about 671 nm is from the $^4F_{9/2}$ energy level of Nd^{3+} under ~1003 nm (Yb^{3+}) emission. As the energy level of the $^4F_{9/2}$ to $^4I_{13/2}$ transition of Nd^{3+} matches with the absorption of Yb^{3+}, it is possible

that a cross-relaxation process would take place. In addition, the excitation peak at around 712 nm is attributed to the $^4F_{7/2}/^4S_{3/2}$ energy level of Nd^{3+} under ~1083 nm (Nd^{3+}) emission. The $^4F_{7/2}/^4S_{3/2}$ is an unstable energy level, the emission from this energy level is highly unlikely to happen. But this energy level can absorb visible light, then relax non-radiatively to $^4F_{3/2}$ energy level. This further proves the rationality of the analysis of the NIR QC process.

Under 264 nm excitation (ascribed to the absorptions of Nd^{3+}-O^{2-} CTB), the emissions around 1000 nm (~ 10 000 cm^{-1}) are dominate, as seen in the inset of Figure 4(a), which are assigned to the $^2F_{5/2}\rightarrow{}^2F_{7/2}$ transitions of Yb^{3+}. This implies NIR QC luminescence in Nd^{3+}/Yb^{3+} co-doped Ca_2SnO_4 occurs. Therefore, the excitation and emission spectra together indicate the presence of NIR QC by a $Nd^{3+}\rightarrow Yb^{3+}$ cross-relaxation energy transfer process. Besides, we can also observe similar emission spectra with Yb^{3+} emission still dominating under 602, 808 nm excitation, but the emissions from Nd^{3+} is significantly enhanced. It shows that only partial energy transfer from Nd^{3+} to Yb^{3+} took place via cross-relaxation. Specially, a marked difference is observed under 808 nm excitation. The emission peak at ~1200 nm is belonged to $^4F_{5/2}$ to $^4I_{13/2}$ transition of Nd^{3+}, because the $^4F_{5/2}$ energy level is always in an excited state upon 808 nm excitation. That is, the electrons are populated at $^4F_{5/2}$ energy level, and emission from this energy level occurs.

The decay curves of $Ca_{1.89}Nd_{0.01}Yb_{0.1}SnO_4$ (λ_{ex}= 264, 602 and 808 nm, λ_{em}= 1003 and 1083 nm) are shown in Figure 4 (b). As can be seen from the decay curves, the lifetime of Yb^{3+} emission is always longer than that of Nd^{3+} emission, no matter under the excitation at Nd^{3+}-O^{2-} CTB or f-f transition absorption of Nd^{3+}. It implies that efficient energy transfer from $Nd^{3+}\rightarrow Yb^{3+}$ probably includes cross-relaxation process.

2.4. The UC red emission of Nd^{3+} in Nd^{3+}/Yb^{3+} co-doped Ca_2SnO_4

The more interesting results are the UC luminescence upon 808 nm laser diode (LD) excitation for Nd^{3+} singly doped and Nd^{3+}/Yb^{3+} co-doped samples. As can be seen, there is no obvious emission in the 400-730 nm for Nd^{3+} singly doped sample $Ca_{1.99}Nd_{0.01}SnO_4$ upon 808 nm LD excitation, curve (i) in Figure 5(a). However, the spectrum is different for the $Ca_{1.89}Nd_{0.01}Yb_{0.1}SnO_4$ sample, a series of emission peaks appear under 808 nm LD excitation, curve (ii) in Figure 5(a). The emission bands are in the 450-550 nm, 575-625 nm and 650-730 nm wavelength ranges, and the UC emission intensity increases with the pumping power(P), Figure 5(b). Here, it needs to be explained that we ignored the emissions in 450-550 nm because of their relatively weak emission intensities compared to other two sets of red emissions with the increase of the pumping power. It indicates that NIR-to-red visible/NIR UC can be realized in Nd^{3+}/Yb^{3+} co-doped Ca_2SnO_4 under 808 nm excitation, which fall within the biological window with potential applications in the bioimaging field.

To further determine the UC mechanism, a plot of logI (I is the total emission intensity) versus logP is illustrated in the inset of Figure 5(b). The fitted slope is 2.35, more closed to 2, which indicates that two-photon processes are involved in producing the UC emission. Therefore, the luminescence process can be schematically described as in Figure 5(c). Under 808 nm LD excitation, the electrons in the $^4I_{9/2}$ ground state of Nd^{3+} absorb the energy and jump to the $^4F_{5/2}$ excited state. The electrons then soon relax to the $^4F_{3/2}$ state and transfer energy to nearby Yb^{3+}ions. Subsequently, the upper levels $^4G_{11/2}$, $^2G_{9/2}$, $^2D_{3/2}$ of Nd^{3+} ions are populated through another cross relaxation process: $^2F_{5/2}$ (Yb^{3+}) + $^4F_{3/2}$ (Nd^{3+}) $\rightarrow$ $^2F_{7/2}$ (Yb^{3+})+ $^4G_{11/2}/^2G_{9/2}/^2D_{3/2}$($Nd^{3+}$). Finally, the UC emission in the 475-550 nm ($^4G_{11/2}$, $^2G_{9/2}\rightarrow{}^4I_{9/2}$;$^4G_{7/2}$, $^4G_{9/2}\rightarrow{}^4I_{9/2}$), 575-625 nm ($^4G_{5/2}$,$^2G_{7/2}\rightarrow{}^4I_{9/2}$;$^4G_{7/2}$, $^4G_{9/2}\rightarrow{}^4I_{11/2}$; $^4G_{11/2}$, $^2G_{9/2}\rightarrow{}^4I_{13/2}$), 650-730 nm ($^4G_{11/2}$, $^2G_{9/2}\rightarrow{}^4I_{15/2}$; $^4G_{7/2}$, $^4G_{9/2}\rightarrow{}^4I_{13/2}$; $^4G_{5/2}$, $^2G_{7/2}\rightarrow{}^4I_{11/2}$; $^4F_{9/2}\rightarrow{}^4I_{9/2}$) wavelength ranges can be observed. Besides, other energy transfer (or cross relaxation) processes such as $^2F_{5/2}$ (Yb^{3+}) + $^4I_{15/2}$ (Nd^{3+}) $\rightarrow$ $^2F_{7/2}$ (Yb^{3+})+ $^4G_{5/2}/^2G_{7/2}$ (Nd^{3+}) may also contribute to the UC process.

Due to the energy transfer from Nd^{3+} to Yb^{3+} and Yb^{3+} to Nd^{3+}, unique UC luminescence from Nd^{3+} occurs in the co-doped samples.

2.5. The NIR QC LLP luminescence in Nd^{3+}/Yb^{3+} co-doped Ca_2SnO_4

We also compared the persistent luminescence of Nd^{3+} singly doped and Nd^{3+}/Yb^{3+} co-doped phosphors. Interestingly, only Nd^{3+}/Yb^{3+} co-doped sample exhibits NIR persistent luminescence. To understand this phenomenon, the thermo-luminescence (TL) curves were measured from the $Ca_{1.99-y}Nd_{0.01}Yb_ySnO_4$ (y = 0.01, 0.03, 0.05, 0.1, 0.15) samples excited by 254 nm source for 5 min.

As an example, the sample with y = 0.1 is shown in Figure 6. Obviously, no peaks exist for $Ca_{1.99}Nd_{0.01}SnO_4$ sample in the temperature range of 50-250 ℃. But when some Yb^{3+} ions were incorporated into the sample, a broad band centered at 90 ℃ appears. The thermal activation energy E of trapped carriers, which corresponds to the trap depth, can be estimated by Hoogenstraaten method. According to the formula,[32]

$$E = 2kT_m^2/\delta \qquad (5)$$

where k is the Boltzmann constant, T_m is the temperature value corresponding to the peak of the TL curve, and $\delta = T - T_m$ (T corresponds to the temperature at half the peak intensity). Using the formula (5), the value of E is 0.80 eV. The results indicate that Yb^{3+} ion can probably act as an electron trap in the host, the presence of Yb^{3+} perhaps contributes to the NIR persistent luminescence. Due to the limitation of experimental instruments, we are unable to obtain more LLP data. But we can still make a reasonable analysis based on the current experimental data. The detailed luminescence mechanism is as follows.

Firstly, we can analyze the generation of traps in the Nd^{3+}/Yb^{3+} co-doped Ca_2SnO_4 compared to the Nd^{3+} singly doped phosphors. As described above about the structure of Ca_2SnO_4, the Ca^{2+} and Nd^{3+} ions are quite similar in their ionic size (i.e., 1.06 and ~1.05 Å, respectively). We present several key discussion points as below: (1) In Nd^{3+} singly doped

Ca_2SnO_4. Nd^{3+} ion can be considered as being doped only at the Ca^{2+} site instead of entering into much smaller Sn^{4+} site as well as the chemical formula $Ca_{1.99}Nd_{0.01}SnO_4$. Furthermore, the Nd^{3+} ions have a trivalent charge, and with the entrance of Nd^{3+} ions into the Ca^{2+} site, Ca vacancies were proposed to maintain charge balance. However, TL test demonstrates that persistent luminescence in Nd^{3+} singly doped system has not been observed. The possible explanation is that Nd^{3+} equally occupies both the Ca^{2+} and Sn^{4+} sites, just like as Eu^{3+} singly doped Ca_2SnO_4.[27] Due to equal substitution, charge compensation exactly cancels out by the path of the following process:

$$Nd_{Nd}^{\times} + Ca_{Ca}^{\times} + Sn_{Sn}^{\times} + Nd_{Nd}^{\times} \rightarrow Nd_{Ca}^{\bullet} + Nd_{Sn}^{'} \quad (6)$$

It should be emphasized here that this is an ideal equivalent replacement, maybe the afterglow is too weak and the instrument cannot respond. (2) In Nd^{3+}/Yb^{3+} co-doped Ca_2SnO_4. It is well known that Yb^{3+} ion has a smaller ionic radius compared to Nd^{3+} or Eu^{3+} because of lanthanide contraction effect. In Nd^{3+}/Yb^{3+} co-doped system, although the nominal chemical formula we designed is $Ca_{1.99}Nd_{0.01}Yb_xSnO_4$, inevitably a part of Yb^{3+} ions maybe occupy smaller Sn^{4+} sites, while Nd^{3+} ions substitute the Ca^{2+} sites. Ca vacancies and several hole traps created by Sn^{4+} site were assumed to keep the charge balance. Apparently, the holes and vacancies stimulate the afterglow emission, as shown in the Figure 6. Hence, NIR LLP luminescence can be obtained in Nd^{3+}/Yb^{3+} co-doped Ca_2SnO_4, especially for the co-doped system at Nd^{3+}/Yb^{3+} with different doping concentration.

Next, the schematic electronic energy levels based on our measured results for Nd^{3+} and Yb^{3+} ions together with band gap and traps in the Ca_2SnO_4 host are illustrated in Figure 7, which can explain the above experimental phenomena. Upon 254 nm excitation, similar to excitation at Nd^{3+}-O^{2-} CTB (~260 nm), strong Yb^{3+} emission together with quite weak Nd^{3+} emission can be observed, as shown in the inset of Figure 4(a).

It is likely that most of the electron absorption energy in the ground state of Nd^{3+} ions is ionized from the $^4I_{9/2}$ to excited state Nd^{3+}-O^{2-} CTB, as denoted by ① step. Since the excited state is very close to the conduction band (CB), electrons are easily captured by the nearby traps level through the CB, denoted by ② step. At the end of 254 nm radiation for 5 min, electrons gradually captured by traps to fill up. Then, the electrons escape from the traps under the action of thermal vibration, which are released back into the CB further Nd^{3+}-O^{2-} CTB, also denoted by ② step. It is considerable that the energy transfer takes place by two-step cross-relaxation processes with ($^4D_{3/2}$) + Yb^{3+} ($^2F_{7/2}$) → Nd^{3+} ($^4G_{5/2}$) + Yb^{3+} ($^2F_{5/2}$) (CR1) and Nd^{3+} ($^4F_{3/2}$) + Yb^{3+} ($^2F_{7/2}$) → Nd^{3+} ($^4I_{9/2}$) + Yb^{3+} ($^2F_{5/2}$) (CR2), and finally produce Yb^{3+} NIR LLP luminescence, denoted by ③ and ④ steps. In these two processes, it demonstrates the occurrence of cross-relaxation energy transfer from the traps level to two Yb^{3+} ions, which exciting both ions from the $^2F_{7/2}$ ground state to the $^2F_{5/2}$ excited state. That is, the NIR QC occurs when the process of traps releasing energy. Combining the above four processes, NIR QC LLP luminescence phosphors will probably occur in Nd^{3+}/Yb^{3+} co-doped Ca_2SnO_4.

At last, we can make an assumption that the electrons escape from the traps due to thermal vibration tunnel through the energy transfer with cooperation to the excited level of the energy-matching of Yb^{3+}, denoted by ⑤ step. In this process, it demonstrates the occurrence of cooperative energy transfer (CET) from the Yb^{3+}-induced traps level to two Yb^{3+} ions, which will greatly improve the yield of QC. The existence of a dopant-induced defect on NIR QC luminescence has been confirmed by the reports[33,34] that Yb^{3+}-doped $CsPb(Cl_{1-x}Br_x)_3$ perovskite thin films with extraordinarily high QC yields reaching >190% by way of CET. This will be our following work. In short, NIR QC LLP luminescence could be achieved by generating NIR luminescence traps through the route of co-doping Yb^{3+} into Ca_2SnO_4: Nd^{3+}.

3. Conclusions

The UC, NIR QC, and NIR QC LLP luminescence in Nd^{3+}/Yb^{3+} co-doped Ca_2SnO_4 phosphors have been investigated via analyzing UC emission spectra, NIR excitation/emission spectra and traps in TL curves. The results indicate that two-photon UC red emission, two-photon NIR QC and NIR QC LLP luminescence can be achieved by the introduction of Yb^{3+} in Ca_2SnO_4: Nd^{3+}. The energy transfer mechanisms of these three luminescent processes is revealed by energy level and decay measurements. For two-photon UC red emission, a cross relaxation process is responsible: $^2F_{5/2}$ (Yb^{3+}) + $^4F_{3/2}$ (Nd^{3+}) $\rightarrow$ $^2F_{7/2}$ (Yb^{3+})+ $^4G_{11/2}/^2G_{9/2}/^2D_{3/2}$($Nd^{3+}$) present under 808 nm laser diode excitation. For two-photon NIR QC, energy transfer occurs from Nd^{3+} to Yb^{3+} via a two-step cross-relaxation: Nd^{3+} ($^4D_{3/2}$) + Yb^{3+} ($^2F_{7/2}$) $\rightarrow$ Nd^{3+} ($^4G_{5/2}$) + Yb^{3+} ($^2F_{5/2}$) and Nd^{3+} ($^4F_{3/2}$) + Yb^{3+} ($^2F_{7/2}$) $\rightarrow$ Nd^{3+} ($^4I_{9/2}$) + Yb^{3+} ($^2F_{5/2}$), and two-step nonradiative relaxation processes: from the level of Nd^{3+}-O^{2-} CTB to $^4D_{3/2}$ and from $^4G_{5/2}$ to $^4F_{3/2}$ upon Nd^{3+}-O^{2-} CTB (~260 nm) excitation. For NIR QC LLP luminescence, similar two-step cross relaxation from the traps level to two Yb^{3+} ions occur upon UV (~254 nm) radiation, equivalent to the NIR QC produced during the process of traps releasing energy. Our work demonstrated that a phosphor with tuning multimode luminescent properties can be obtained as Nd^{3+} activated Ca_2SnO_4 induced by Yb^{3+}. Ca_2SnO_4: Nd^{3+}, Yb^{3+} NIR luminescent materials with multimodal functions can expect to give applications in many important areas, especially in biomedical imaging and crystalline Si solar cells fields.

4. Experimental Section

Instrumentation: Phase identification of the obtained products was analyzed by means of a Philips PW1830 X-ray powder diffractometer (XRD) using graphite monochromator and Cu Kα (λ = 1.54056Å) radiation at 40 kV and 40 mA. Steady state photoluminescence (PL) spectra were recorded on an Edinburgh FLS920 spectrofluorimeter where a continuous wave

450 W xenon lamp was used as the excitation source, and the infrared emission was detected by a liquid-nitrogen cooled R5509-72 NIR photomultiplier tube (PMT). Besides, dynamic fluorescence spectra like decay curves were recorded with microsecond μF900 xenon lamp excitation sources. UC emission spectra were recorded on the Jobin-Yvon TRIAX320 spectrofluorimeter equipped with a R928 photomultiplier tube as the detector and an 808 nm laser diode (LD, Coherent Corp.) as monochromatic light source. Thermoluminescence (TL) glow curves were measured with a FJ-427A TL meter (Beijing Nuclear Instrument Factory) by heating the irradiated samples from 313 to 473 K. The samples were pre-irradiated by using a 254 Xe lamp for 5 min and then heated at a linear rate of 2 $K \cdot s^{-1}$ to release the energy reserved in the material. TL signals were recorded in the temperature range of 273−773 K and the heating rate was fixed at 5 $K \cdot s^{-1}$. All the PL spectra were corrected for the wavelength-dependent response of the detector system. For comparison, the spectra were recorded under identical measurement conditions. Appropriate optical filters were employed to avoid any possible interference in all spectral measurements. All measurements were carried out at room temperature.

Experimental Procedures: The Nd^{3+} and Yb^{3+} doped Ca_2SnO_4 phosphors were prepared by conventional high temperature solid state reaction method, the raw materials are $CaCO_3$ (A. R.), SnO_2 (A. R.), Nd_2O_3 (99.99%), Yb_2O_3(99.99%). The stoichiometric starting materials were ground in an agate mortar and heated at 750 ºC for 1 hour. After cooling down to room temperature (RT), the as-obtained powders were reground and then calcined at 1350 ºC for 6 hours in air atmosphere to obtain the final products.

Acknowledgements

This work is supported by the National Natural Science Foundation of China (No. 21301043), Natural Science Foundation of Guangdong Province (No. 2018A030313081), Guangdong Basic and Applied Basic Research Foundation (Nos. 2020A1515011403, 2020A1515011188),

The Innovation Team Program of Higher Education of Guangdong, China (No. 2017KCXTD023), Characteristic innovation projects of Guangdong Provincial Department of Education (No. 2018KTSCX137).

References

[1] D.J. Naczynski, M.C. Tan, M. Zevon, B. Wall, J. Kohl, A. Kulesa, S. Chen, C.M. Roth, R.E. Riman, P.V. Moghe, *Nat. Commun.* **2013**, 4, 3199.

[2] D. Yu, R. Martín-Rodríguez, Q. Zhang, A. Meijerink, F.T. Rabouw, *Light Sci. Appl.* **2015**, 4, e344.

[3] T. Yu, H. Lin, D. Yu, S. Ye, Q. Zhang, *J. Phys. Chem. C* **2015**, 119, 26643.

[4] Y. Ma, J. Bao, Y. Zhang, Z. Li, X. Zhou, C. Wan, L. Huang, Y. Zhao, G. Han, T. Xue, *Cell* **2019**, 177, 1.

[5] H. Zeng, T. Zhou, L. Wang, R.-J. Xie, *Chem. Mater.* **2019**, 31, 5245.

[6] P. Vergeer, T. J. H. Vlugt, M. H. F. Kox, M. I. den Hertog, J. P. J. M. van der Eerden, A. Meijerink, *Phys. Rev. B* **2005**, 71, 014119.

[7] van der Ende B. M., L. Aarts, A. Meijerink, *Adv. Mater.* **2009**, 21, 3073.

[8] D. Yu, T. Yu, Y. Wang, Q. Zhang, A. Meijerink, *Phys. Rev. Appl.* **2020**, 13, 024076.

[9] F. Liu, Y. Liang, Z. Pan, *Phys. Rev. Lett.* **2014**, 113, 177401.

[10] T. Maldiney, A. Bessière, J. Seguin, E. Teston, S. K. Sharma, B. Viana, A. J. J. Bos, P. Dorenbos, M. Bessodes, D. Gourier, D. Scherman, C. Richard, *Nat. Mater.* **2014**, 13, 418.

[11] Z. Zou, L. Feng, C. Cao, J. Zhang, Y. Wang, *Sci. Rep.* **2016**, 6, 24884.

[12] X. Zhou, W. Geng, J. Li, Y. Wang, J. Ding, Y. Wang, *Adv. Optical Mater.* **2020**,1902003.

[13] W.-T. Huang, C.-L. Cheng, Z. Bao, C.-W. Yang, K.-M. Lu, C.-Y. Kang, C.-M. Lin, R.-S. Liu, *Angew. Chem.* **2019**, 131, 2091.

[14] G. Blasse, B. C. Grabmaier, *Luminescent Materials* Springer-Verlag press, Berlin, 1994, p. 26.

[15] R. J. R. Vieira, L. Gomes, J. R. Martinelli, N. U. Wetter, *Opt. Express* **2012**, 20, 12487.

[16] D. Jaque, J. García Solé, *Phys. Rev. B* **2004**, 70, 155116.

[17] I. Mikalauskaite, G. Pleckaityte, L. Sinusaite, V. Plausinaitiene, A. Katelnikovas, A. Beganskiene, *J. Lumin.* **2020**, 223, 117237.

[18] J. Ueda, T. Shinoda, S. Tanabe, *Opt. Mater. Express* **2013**, 3, 787.

[19] Y. Teng, J. Zhou, Z. Ma, M. M. Smedskjaer, J. Qiu, *J. Electrochem. Soc.* **2011**, 158, K17.

[20] H. Lin, T. Yu, M.-K. Tsang, G. Bai, Q. Zhang, J. Hao, *Appl. Phys. Lett.* **2016**, 108, 041902.

[21] H. Lin, T. Yu, G. Bai, M-K. Tsang, Q. Zhang, J. Hao, *J. Mater. Chem. C* **2016**, 4, 3396.

[22] X. Zhang, J. Zhao, B. Chen, T. Sun, R. Ma, Y. Wang, H. Zhu, D. Peng, F. Wang, *Adv. Optical Mater.* **2020**, 2000274.

[23] A. Yakovliev, T. Y. Ohulchanskyy, R. Ziniuk, T. Dias, X. Wang, H. Xu, G.Y. Chen, J.L. Qu, S. L. Anderson, *Part. Part. Syst. Charact.* **2020**, 1900445.

[24] S. Li, Y. Xia, M. Amachraa, N. Hung, Z. Wang, S. Ong, R.-J. Xie, *Chem. Mater.* **2019**, 31, 6286.

[25] R.D.Shannon, *Acta Crystallogr.* **1976**, A32, 751.

[26] T. Ishigaki, A. Torisaka, K. Nomizu, P. Madhusudan, K. Uematsu, K. Toda, M. Sato, *Dalton Trans.* **2013**, 42, 4781.

[27] Y. Fujimichi, S.Muto, K.Tatsumi, T.Kawano, H.Yamane, *J. Solid State Chem.* **2010**, 183, 2127.

[28] H. Yamane, Y. Kaminaga, S. Abe, T. Yamada, *J. Solid State Chem.* **2008**, 181, 2559.

[29] S. Kamimura, C. N. Xu, H. Yamada, N. Terasaki, M. Fujihala, *Jpn. J. Appl. Phys.* **2014**, 53, 092403.

[30] P. Dorenbos, *J. Phys.: Condens. Matter* **2003**, 15, 8417.

[31] H. Lin, H. Liang, B. Han, J. zhong, Q. Su, P. Dorenbos, M.Danang Birowosuto, G. Zhang, Y. Fu, W. Wu, *Phys. Rev. B* **2007**, 76(3), 035117.

[32] F. You, A. J. J. Bos, Q. Shi, S. Huang, P. Dorenbos, *Phys. Rev. B* **2012**, 85, 115101.

[33] D. M. Kroupa, J. Y. Roh, T. J. Milstein, S. E. Creutz, D. R. Gamelin, *ACS Energy Lett.* **2018**, 3, 2390.

[34] T. J. Milstein, D. M. Kroupa, D. R. Gamelin, *Nano Lett.* **2018**, 18, 3792.

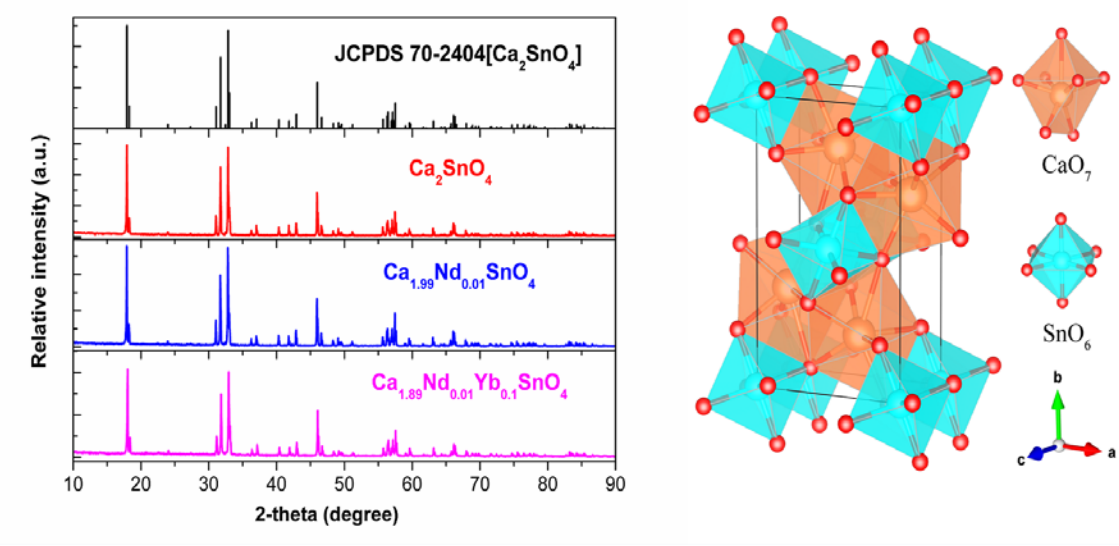

Figure 1. (a) XRD patterns of the samples Ca_2SnO_4, $Ca_{1.99}Nd_{0.01}SnO_4$, and $Ca_{1.89}Nd_{0.01}Yb_{0.1}SnO_4$. (b) Schematic diagram of Ca_2SnO_4 structure and coordination environment of the Ca^{2+}, and Sn^{4+} cations.

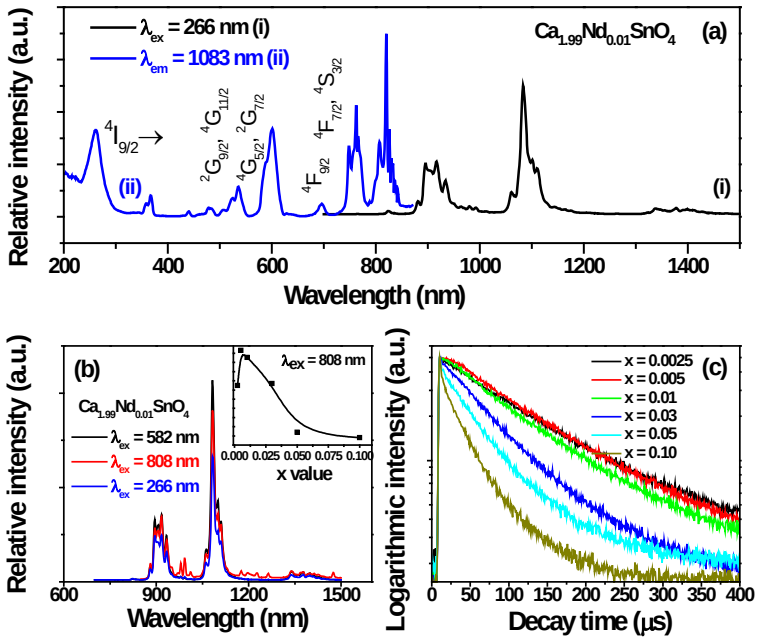

Figure 2. (a) The emission (i) and the excitation (ii) spectra of $Ca_{1.99}Nd_{0.01}SnO_4$ at room temperature. (b) The emission spectra of $Ca_{1.99}Nd_{0.01}SnO_4$ sample under 266 nm, 582 nm and 808 nm excitation; inset is the emission intensity as a function of Nd^{3+} concentration under 808 nm excitation. (c) The decay curves of $Ca_{2-x}Nd_xSnO_4$(x = 0.0025, 0.005, 0.01, 0.03, 0.05, 0.1) (λ_{ex}= 808 nm, λ_{em}= 1083 nm).

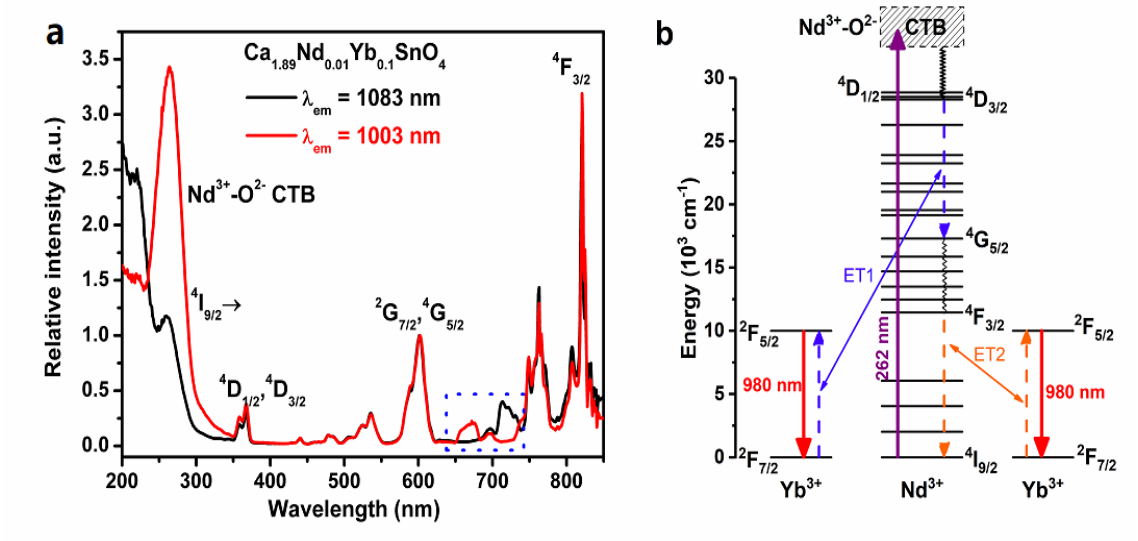

Figure 3. (a) The excitation spectra of $Ca_{1.89}Nd_{0.01}Yb_{0.1}SnO_4$ (λ_{em}= 1003 nm and 1083 nm). (b) Energy-level diagram schematically illustrating the proposed energy transfer mechanisms of two-photon NIR QC in Nd^{3+}/Yb^{3+} co-doped Ca_2SnO_4.

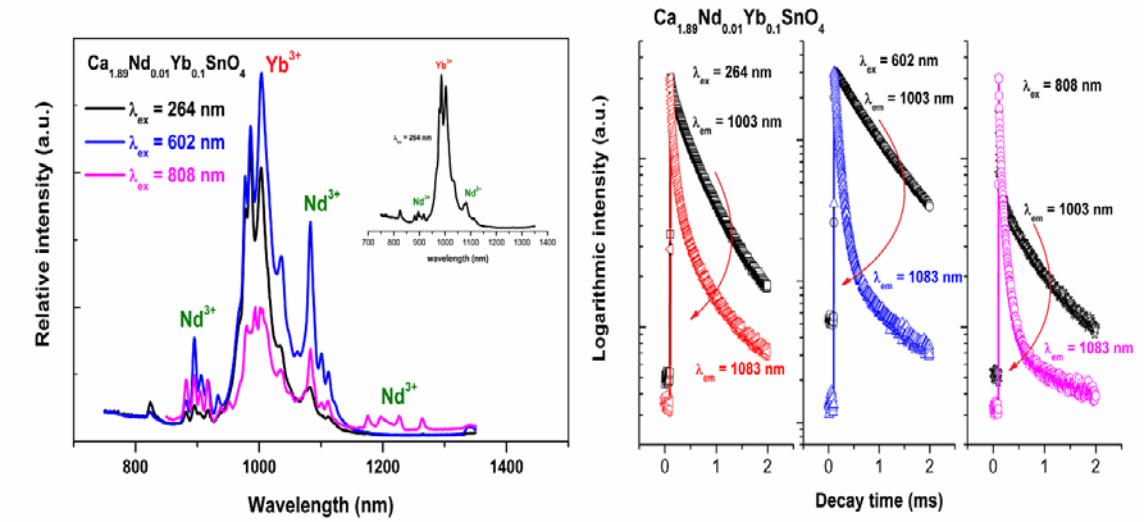

Figure 4. (a) The emission spectra of $Ca_{1.89}Nd_{0.01}Yb_{0.1}SnO_4$ (λ_{ex}= 264, 602 and 808 nm), the inset is the emission spectrum under 264 nm excitation. (b) The decay curves of $Ca_{1.89}Nd_{0.01}Yb_{0.1}SnO_4$ (λ_{ex}= 264, 602 and 808 nm, λ_{em}= 1003 and 1083 nm).

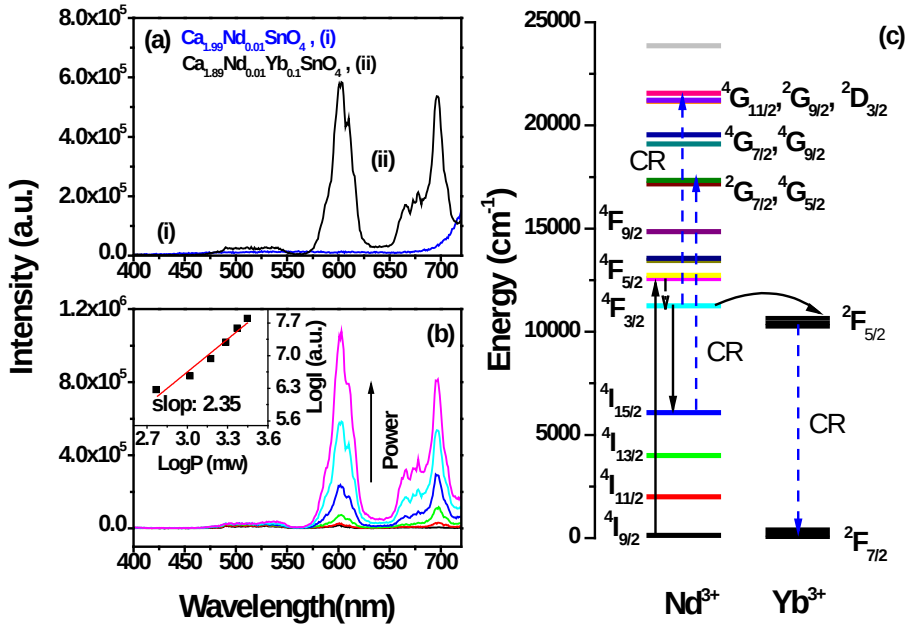

Figure 5. (a) The emission spectra of $Ca_{1.99}Nd_{0.01}SnO_4$ and $Ca_{1.89}Nd_{0.01}Yb_{0.1}SnO_4$ under 808 nm excitation. (b) The emission spectra at different pumping power. The inset is the pumping power dependence of the upconversion emission intensity under 808 nm excitation. (c) Energy level diagram and the possible UC luminescence mechanism.

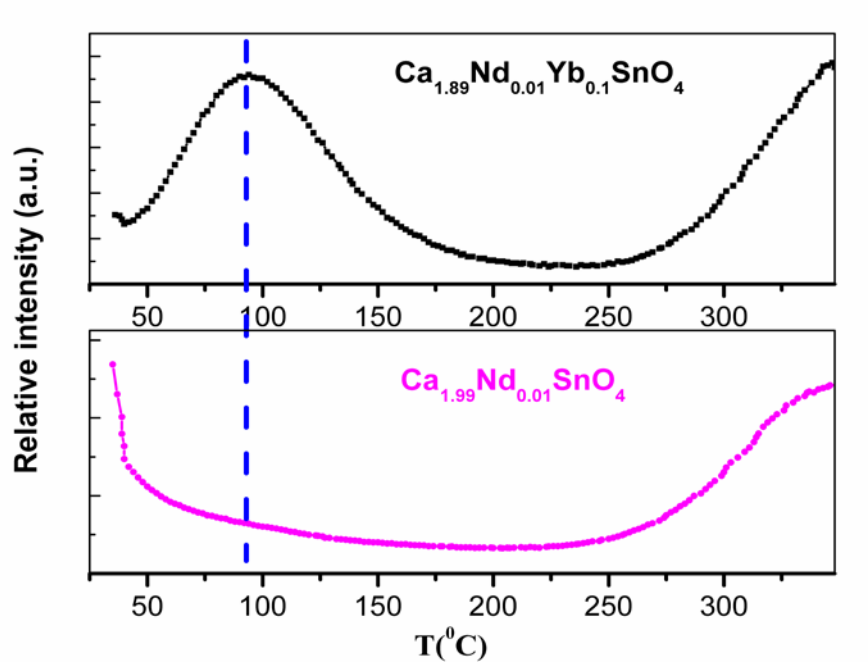

Figure 6. The thermo-luminescence curves of $Ca_{1.99}Nd_{0.01}SnO_4$ and $Ca_{1.89}Nd_{0.01}Yb_{0.1}SnO_4$ samples.

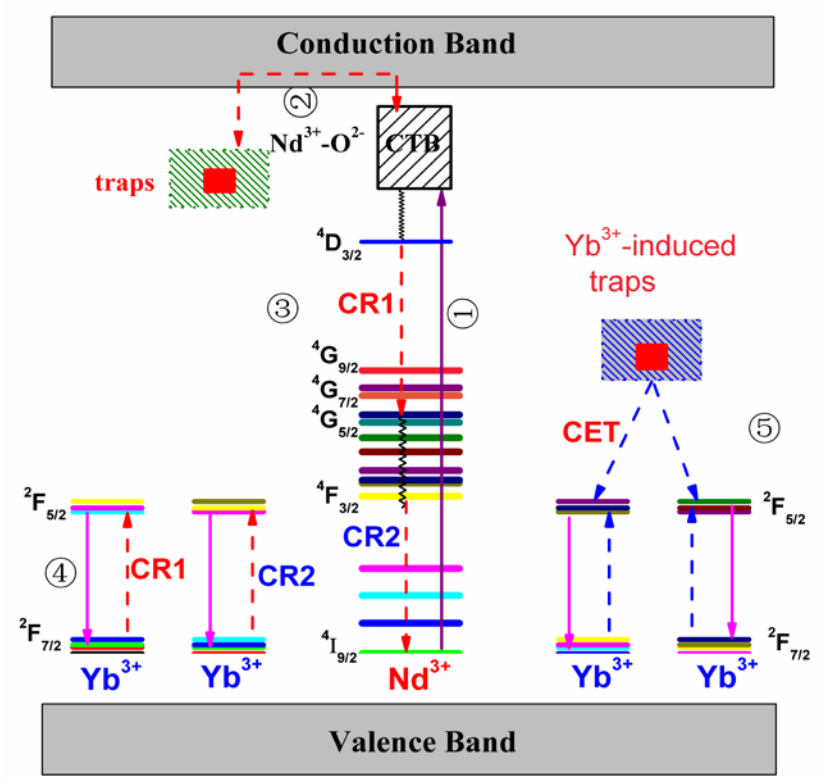

Figure 7. Energy-level diagram schematically illustrating the proposed energy transfer mechanisms of two-photon NIR QC LLP in Nd^{3+}/Yb^{3+} co-doped Ca_2SnO_4.

ToC figure